Increasing the performance of active noise control systems on ground with two vertical reflecting surfaces with an included angle

Jiaxin Zhong,[1] Jiancheng Tao,[1,a)] and Xiaojun Qiu[2]
[1]*Key Laboratory of Modern Acoustics, Institute of Acoustics, Nanjing University, Nanjing 210093, China*
[2]*Centre for Audio, Acoustics and Vibration, Faculty of Engineering and Information Technology, University of Technology Sydney, New South Wales 2007, Australia*

(Received 20 March 2019; revised 22 October 2019; accepted 27 October 2019; published online 3 December 2019)

This paper investigates the feasibility of increasing the noise reduction performance of active noise control (ANC) systems on ground by introducing two vertical reflecting surfaces with an included angle. By using the image source method, the theory of sound wave propagation in a wedge-shaped reflector and the integral equation method, the noise reduction of the ANC systems with two infinitely large or finite size reflecting surfaces with different included angles are studied. It is demonstrated that the noise reduction of the system can be increased significantly with two reflecting surfaces after optimizing their included angle and size. The simple empirical formulas for the optimal included angle of the surfaces and the noise reduction are presented. It is found that the noise reduction at 500 Hz increases by 13.6 dB when two vertical reflecting surfaces are arranged with an optimal angle of 125° and the source distance is 0.1 m. By optimizing the size of the reflecting surfaces to about 0.35 of the wavelength, the noise reduction can be further increased by approximately 2.8 dB. The mechanisms for the performance improvement are disclosed, and the experiments are conducted to validate the results.
https://doi.org/10.1121/1.5134062

[SKT] Pages: 4075–4085

I. INTRODUCTION

In some applications of active sound radiation control, there exist vertical reflecting surfaces around the system, such as the fire barrier walls around power transformers. These reflecting surfaces and the ground affect the radiation pattern of the sources and the noise reduction performance of active noise control (ANC) systems.[1] However, the effects of two reflecting surfaces with an included angle on ANC systems on ground are rarely studied.[2]

The ground is typically regarded as an infinitely large rigid plane, and its effects on the noise reduction of ANC systems for sound radiation control have been widely investigated by the image source method.[3,4] For single channel ANC systems, ground reflection can increase the noise reduction if the primary and secondary sources are placed along a line vertical to the ground.[5] The mechanism is that the point monopole (primary source) controlled by one secondary source at low frequency can be approximately considered as a dipole source, and the ground converts a dipole-like source vertical to the ground into a longitudinal quadrupole.[6] After introducing a finite size reflecting surface vertical to the ground, the noise reduction of the system can be further increased.[7]

For an extended primary source whose characteristic dimensions are comparable to the wavelength, the noise reduction of the ANC system is also affected by the ground if the geometric center of the source is within 1/5 of the wavelength from the ground.[8] For multichannel ANC systems on ground, the noise reduction can be maximally increased if the secondary sources are placed as far apart as possible from each other and the ground.[9] The mechanism is that the additional reflecting surface produces more image secondary sources, which can enhance the performance of ANC systems.

The performance of active control systems near two vertical reflecting surfaces has been studied with numerical simulations, where the included angle between the two surfaces is 90°.[10] Numerical results show that the noise reduction of the ANC system depends on the elevation angle, the azimuth angle, and the distances between the sources and surfaces. If two reflecting surfaces are optimally placed, higher noise reduction of the ANC system can be achieved compared with the case with only one reflecting surface. The mechanism for the noise reduction enhancement is the change of the acoustic impedance caused by the reflecting surfaces. However, the two reflecting surfaces with different included angles have not been considered, and there has been no experimental validation until now.

The vertically placed wedge-shaped reflector on ground is used in this paper to study the effects of two reflecting surfaces with an included angle ranging from 0° to 180°. When the size of the reflector is infinitely large, the sound propagation in a wedge-shaped reflector can be solved with separation of variables in a cylindrical coordinate system.[11,12] When the size of the reflector is finitely large, no analytical solution is available, but the sound field can be calculated

a)Electronic mail: jctao@nju.edu.cn

using the finite element method (FEM) or other integral equation methods.[13]

This paper investigates the feasibility of increasing the noise reduction of a single channel ANC system on ground by introducing two vertically placed reflecting surfaces with an included angle. The maximal noise reduction of the ANC system inside a wedge-shaped reflector is calculated first, then the formulas of the optimal included angle of the reflector and the noise reduction below the controlling frequency are derived analytically, and their simpler empirical formulas are presented. The optimal size of the wedge-shaped reflector is then investigated based on the integral equation method. The mechanisms for the performance improvement are disclosed, and the experimental results are presented to validate the analytical and simulation results.

II. THEORETICAL ANALYSES

Figure 1 shows an ANC system on ground with two vertically placed reflecting surfaces. The reflecting surfaces can be infinitely large or with a width of w and a height of h, and the included angle of the two surfaces is θ. A cylindrical coordinate system (ρ,φ,z) is established, centered at the intersection of the reflectors and the ground. The ground plane is at $y=0$, so the location of the image source from the ground for a sound source located at (ρ,φ,z) is $(\rho,\varphi,-z)$. When the source is on the ground plane ($z=0$), the point monopole and its image coincide. The distance between the primary and secondary sources is d, and the distance between the secondary source and the coordinate origin O is l.

A. Sound field with two infinitely large reflecting surfaces

The vertically placed infinitely large wedge-shaped reflector on ground is considered first because its sound field can be solved analytically.[11,12] By using the image source method, the sound pressure at $\mathbf{r} = (\rho,\varphi,z)$ generated by a point monopole at $\mathbf{r}_0 = (\rho_0,\varphi_0,z_0)$ is expressed as the superposition of the sound pressure of the source and its image,

$$p(\mathbf{r};\mathbf{r}_0) = -\mathrm{j}\rho_{\mathrm{air}}\omega q_0[G(\mathbf{r};\rho_0,\varphi_0,z_0;\theta) + G(\mathbf{r};\rho_0,\varphi_0,-z_0;\theta)], \quad 0 \le \varphi, \ \varphi_0 \le \theta, \tag{1}$$

where j is the imaginary unit, ρ_{air} is the air density, ω is the angular frequency of the sound emitted by the source, the time varying component $e^{-\mathrm{j}\omega t}$ is omitted, q_0 is the source strength, and $G(\mathbf{r};\mathbf{r}_0;\theta)$ is the Green function inside the infinitely large wedge-shaped reflector without the ground, which can be expressed in the form[11]

$$G(\mathbf{r};\mathbf{r}_0;\theta) = \frac{\mathrm{j}k}{2\theta}\sum_{m=0}^{\infty}\sum_{n=0}^{\infty}\frac{\varepsilon_m(k\rho\rho_0/2)^{2n+m\pi/\theta}}{n!\Gamma(n+m\pi/\theta+1)} \times \cos\left(\frac{m}{\theta}\pi\varphi_0\right)\cos\left(\frac{m}{\theta}\pi\varphi\right) \times \frac{h^{(1)}_{2n+m\pi/\theta}\left(k\sqrt{\rho^2+\rho_0^2+(z-z_0)^2}\right)}{\left[\sqrt{\rho^2+\rho_0^2+(z-z_0)^2}\right]^{2n+m\pi/\theta}}, \tag{2}$$

where k is the wavenumber, ε_m is the Neumann factor, i.e., $\varepsilon_m = 1$ ($m=0$) and $\varepsilon_m = 2$ ($m = 1, 2, 3, \ldots$), $\Gamma(\cdot)$ is the gamma function, and $h_m^{(1)}(\cdot)$ is the spherical Hankel function of the first kind of order m.

The sound radiation power of an ANC system consisting of a primary source and one secondary source can be formulated as[14]

$$W = A|q_{\mathrm{s}}|^2 + q_{\mathrm{s}}^* b + b^* q_{\mathrm{s}} + c, \tag{3}$$

where q_{s} is the complex source strength of the secondary source, "*" denotes complex conjugation, $A=0.5Z_{\mathrm{s}}$, Z_{s} is the self-radiation resistance of the secondary source, $b=0.5q_{\mathrm{p}}Z_{\mathrm{ps}}$, Z_{ps} is the mutual radiation resistance between the primary source and the secondary source, $c=0.5|q_{\mathrm{p}}|^2Z_{\mathrm{p}}$, and q_{p} and Z_{p} are the complex source strength and the self-radiation resistance of the primary source, respectively. These resistances can be obtained by using Eq. (1) as

$$Z_{\mathrm{p}} = \mathrm{Re}\left[p(\mathbf{r}_{\mathrm{p}};\mathbf{r}_{\mathrm{p}})/q_{\mathrm{p}}\right], \tag{4}$$

$$Z_{\mathrm{s}} = \mathrm{Re}\left[p(\mathbf{r}_{\mathrm{s}};\mathbf{r}_{\mathrm{s}})/q_{\mathrm{s}}\right], \tag{5}$$

$$Z_{\mathrm{ps}} = \mathrm{Re}\left[p(\mathbf{r}_{\mathrm{p}};\mathbf{r}_{\mathrm{s}})/q_{\mathrm{s}}\right], \tag{6}$$

where Re[·] denotes the real part of the quantity inside the square brackets.

After obtaining the optimal secondary source strength,[14]

$$q_{\mathrm{s,opt}} = -\frac{Z_{\mathrm{ps}}}{Z_{\mathrm{s}}}q_{\mathrm{p}}. \tag{7}$$

The minimal sound radiation power under optimal control is

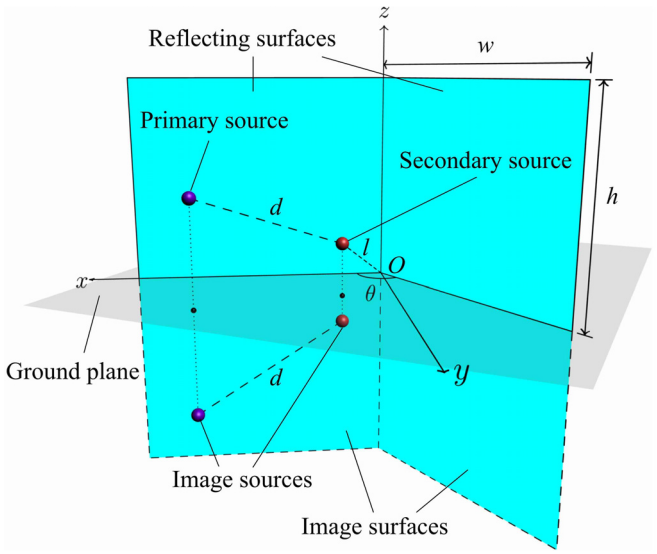

FIG. 1. (Color online) Schematic diagram of an active noise control (ANC) system on ground with two vertically placed reflecting surfaces with an included angle θ.

$$W_{\text{opt}} = \frac{1}{2}|q_{\text{p}}|^2\left(Z_{\text{p}} - \frac{Z_{\text{ps}}^2}{Z_{\text{s}}}\right). \tag{8}$$

The noise reduction is defined as

$$\text{NR} \equiv -10\lg\left(\frac{W_{\text{opt}}}{W_0}\right), \tag{9}$$

where the sound radiation power of the primary source on ground $W_0 = (\rho_{\text{air}}\omega k|q_{\text{p}}|^2)/(4\pi)$ is used as the reference. This defined noise reduction is 0 dB without ANC if there are no additional reflecting surfaces around the system. For a constant volume primary source on ground, its sound radiation power (without ANC) varies after introducing reflecting surfaces near it. For example, its sound radiation power is increased by 3 dB when an infinitely large reflecting surface is introduced against the primary source at the low frequency. Therefore, the NR defined by Eq. (9) can then be nonzero (or even negative) without ANC when there are additional reflecting surfaces around it.

B. Optimal angle of the infinitely large reflecting surfaces

Substitute Eq. (8) into Eq. (9), and the noise reduction can be written in terms of the resistances as

$$\text{NR} = -10\lg\left(\frac{2\pi}{\rho_{\text{air}}\omega k}\frac{Z_{\text{p}}Z_{\text{s}} - Z_{\text{ps}}^2}{Z_{\text{s}}}\right). \tag{10}$$

The equation shows that the noise reduction increases when the term $(Z_{\text{p}}Z_{\text{s}} - Z_{\text{ps}}^2)/Z_{\text{s}}$ decreases. According to the reciprocity theorem, the value of $(Z_{\text{p}}Z_{\text{s}} - Z_{\text{ps}}^2)$ does not change if the location of the primary and secondary sources is exchanged.[14] But the value of Z_{s} might change after the exchanging operation. High noise reduction can be obtained if the secondary source is positioned in a place where it has high self-radiation resistance. Therefore, when a wedge-shaped reflector is introduced near a single channel ANC system, the reflector should be placed close to the secondary source to increase the self-radiation resistance of the secondary source.

Under optimal control for two closely located primary and secondary sources, the secondary source is usually unloaded, so its sound radiation power is quite small, and the total sound radiation power of the system is mainly determined by the mutual radiation power of the primary source from the secondary source and the self-radiation power of the primary source.[9] Therefore, the primary source should be placed as far as possible from both reflecting surfaces so that the self-radiation of the primary source is small. This implies the line of the primary and secondary sources is on the bisector of the two reflecting surfaces of the wedge-shaped reflector.

Although there are many different geometry configurations for the primary and secondary sources, this paper only focuses on a specific configuration where the primary and secondary sources are located on ground and the bisector of the wedge-shaped reflector with the reflector are placed close to the secondary source, as shown in Fig. 1. When the secondary source is located at the intersection of the wedge-shaped reflector and the ground, the self-radiation resistance of the secondary source and the mutual radiation resistance between the two sources can be simplified using Eqs. (1), (5), and (6) as

$$Z_{\text{s}} = \frac{\rho_{\text{air}}\omega k}{\theta}, \quad Z_{\text{ps}} = \frac{\rho_{\text{air}}\omega k}{\theta}\text{sinc}(kd), \tag{11}$$

where the function $\text{sinc}(x) = \sin(x)/x$. The self-radiation resistance of the primary source, obtained using Eqs. (1) and (4), is complicated but can be expanded at low frequency as

$$\begin{aligned} Z_{\text{p}} = \frac{\rho_{\text{air}}\omega k}{\theta}\Bigg[1 &- \frac{1}{3}(kd)^2 + \frac{1}{20}(kd)^4 - \frac{1}{252}(kd)^6 \\ &+ \frac{2}{\Gamma(4\pi/\theta+2)}(kd)^{4\pi/\theta} + \frac{2(4\pi/\theta+2)}{\Gamma(4\pi/\theta+4)}(kd)^{4\pi/\theta+2} \\ &+ o((kd)^6)\Bigg], \end{aligned} \tag{12}$$

where $o(\cdot)$ represents the higher order of the variable inside the parenthesis. The minimal sound radiation power of the system is then obtained by substituting Eqs. (11) and (12) into Eq. (8),

$$\begin{aligned} W_{\text{opt}} = \frac{\rho_{\text{air}}\omega k|q_{\text{p}}|^2}{2\theta}\Bigg[&\frac{1}{180}(kd)^4 - \frac{1}{1260}(kd)^6 \\ &+ \frac{2}{\Gamma(4\pi/\theta+2)}(kd)^{4\pi/\theta} + \frac{2(4\pi/\theta+2)}{\Gamma(4\pi/\theta+4)}(kd)^{4\pi/\theta+2} \\ &+ o((kd)^6)\Bigg]. \end{aligned} \tag{13}$$

By truncating the orders not less than $(kd)^6$ of the above equation, the noise reduction can be simplified by substituting Eq. (13) into Eq. (9),

$$\text{NR} = -10\lg\left[\frac{\pi}{90\theta}(kd)^4 + \frac{4\pi}{\theta\Gamma(4\pi/\theta+2)}(kd)^{4\pi/\theta}\right]. \tag{14}$$

When $4\pi/\theta > 6$, i.e., $0 < \theta < 2/3\pi$, the second term inside the logarithm function in Eq. (14) can be omitted, and the noise reduction can be further simplified as

$$\text{NR} = -10\lg\left[\frac{\pi}{90\theta}(kd)^4\right]. \tag{15}$$

Equation (15) shows that the noise reduction of the system at low frequency, i.e., kd is small, is larger than that of the system for a single channel system in free field, which is known as $\text{NR} = -10\lg[(kd)^2/3]$.[15]

By taking the derivative of Eq. (14) with respect to the angle and letting it be equal to zero, one finds that the optimal angle θ_{opt} satisfies

$$\frac{1}{360}(kd)^{4-4\pi/\theta_{\text{opt}}} = \frac{4\pi\psi(4\pi/\theta_{\text{opt}}+2) - \theta_{\text{opt}} - 4\pi\ln(kd)}{\theta_{\text{opt}}\Gamma(4\pi/\theta_{\text{opt}}+2)}, \tag{16}$$

where $\psi(x) \equiv (d\ln[\Gamma(x)])/dx$ is the digamma function.[16] Equation (16) is a little bit complicated to have an analytic solution, and one empirical formula is proposed as

$$\theta_{\text{opt}} = 146^\circ - 133^\circ \frac{kd}{2\pi}, \tag{17}$$

provided that the source interval, d, is less than one-quarter of the corresponding wavelength. The numerical results show that the maximal error of the empirical formula is less than 5°.

C. Sound field with two finite size reflecting surfaces

For practical situations when the width and height of the wedge-shaped reflector are finite, the sound field can be solved based on the integral method.[13] Similar to the model described in Ref. 12, a virtual boundary S is assumed. The whole space above the ground is then divided into two regions denoted by region I ($0 \le \varphi \le \theta$ and $z \ge 0$) and region II ($\theta \le \varphi \le 2\pi$ and $z \ge 0$). The sound field in region I where the sound source location is determined by the continuous boundary conditions on the virtual boundary S.

Following the Kirchhoff-Helmholtz equation, the sound pressure at location $\mathbf{r}$ due to a point monopole at location $\mathbf{r}_0$ in region I can be written as

$$p^{\text{I}}(\mathbf{r}) = -\text{j}\rho_{\text{air}}\omega q_0 G^{\text{I}}(\mathbf{r};\mathbf{r}_0) + \int\int_S G^{\text{I}}(\mathbf{r};\mathbf{r}')\frac{\partial p^{\text{I}}(\mathbf{r}')}{\partial n}dS', \tag{18}$$

where $\partial/\partial n$ represents the directional derivative on the virtual boundary toward region II. Similarly, the sound pressure at location $\mathbf{r}$ in region II can be written as

$$p^{\text{II}}(\mathbf{r}) = -\int\int_S G^{\text{II}}(\mathbf{r};\mathbf{r}')\frac{\partial p^{\text{II}}(\mathbf{r}')}{\partial n}dS'. \tag{19}$$

The Green functions in regions I and II are obtained by using the image source method as

$$G^{\text{I}}(\mathbf{r};\mathbf{r}_0) = G(\mathbf{r};\mathbf{r}_0;\theta) + G(\mathbf{r};\rho_0,\varphi_0,-z_0;\theta), \quad 0 \le \varphi,\ \varphi_0 \le \theta, \tag{20a}$$

$$G^{\text{II}}(\mathbf{r};\mathbf{r}_0) = \sum_{i=0,1} G(\rho,\varphi-\theta,z;\rho_0,\varphi_0-\theta,(-1)^i z_0;2\pi-\theta), \quad \theta \le \varphi,\ \varphi_0 \le 2\pi, \tag{20b}$$

where $G(\mathbf{r};\mathbf{r}_0;\theta)$ is defined in Eq. (2).

The continuous conditions on the virtual boundary S are[13]

$$p^{\text{I}}(\mathbf{r}')|_S = p^{\text{II}}(\mathbf{r}')|_S, \tag{21a}$$

$$\left.\frac{\partial p^{\text{I}}(\mathbf{r}')}{\partial n}\right|_S = \left.\frac{\partial p^{\text{II}}(\mathbf{r}')}{\partial n}\right|_S \equiv f(\mathbf{r}'). \tag{21b}$$

Therefore, it has the relation

$$\int\int_S [G^{\text{I}}(\mathbf{r};\mathbf{r}') + G^{\text{II}}(\mathbf{r};\mathbf{r}')]f(\mathbf{r}')dS' = \text{j}\rho_{\text{air}}\omega q_0 G^{\text{I}}(\mathbf{r};\mathbf{r}_S), \tag{22}$$

where only the pressure derivative on the virtual boundary $f(\mathbf{r}')$ is unknown. The sound pressure in region I can be calculated using Eq. (17) after $f(\mathbf{r}')$ is obtained by solving Eq. (22). A numerical scheme similar to that in Ref. 12 is utilized to solve Eq. (22), but the detail is not presented in this paper for concision. After the sound pressure at any point inside the wedge-shaped reflector is solved, one can obtain the sound power of the ANC system by using Eqs. (3)–(6).

III. SIMULATIONS

The specific configuration discussed in Sec. II is considered where the primary and secondary sources are located on the ground and the bisector of the wedge-shaped reflector. The reflector is placed close to the secondary source. In order to keep the effects of the reflector on the radiation of the primary source the same for all cases, the distance between the primary source and the intersection of the ground and the reflector is set to 0.1 m throughout the simulations. The frequency of interest ranges from 315 Hz to 5 kHz.

Figure 2 shows the noise reduction of the ANC system when the reflector is at different distances from the secondary source. It is clear that installing the reflector closer to the secondary source usually provides better noise reduction performance in the low frequency range. The noise reduction of the system can be smaller than that without the reflector at some frequencies, for example, around 1000 Hz when the included angle of the reflector is 30° and the distance between the secondary source and the reflector is not 0. This is because the radiation resistance of the primary source is increased by the additional reflecting surfaces while the effects of the ANC are relatively weak.

To focus on the effects of the included angle of the reflector, the distance between the secondary source and the reflector, l, is set to 0 in the following simulations. Figure 3 shows the noise reduction of the ANC system with different included angles. It can be found that the noise reduction is increased significantly at the low frequencies after the reflector is introduced depending on the included angle. For example, the noise reduction at 500 Hz without the reflector is 6.0 dB, and it can be further increased by 7.8 dB, 12.5 dB, 13.6 dB, or 9.6 dB after the reflector is introduced with the included angle θ being 30°, 90°, 120° or 180°, respectively.

There is an optimal included angle of the reflector to have the maximum noise reduction. Figure 4 shows the noise reduction of the system under the optimal control at 500 Hz with the included angle ranging from 1° to 180°. The noise reduction of the ANC system increases with the angle first and then decreases after it reaches the maximal value 19.6 dB at 125°. The maximal noise reduction of the ANC system at this optimal angle is 1.1 dB and 4.0 dB higher than those of the two typical configurations with the angle 90° and 180°, respectively. Figure 4 also shows that the noise reduction curve can be estimated by using the simple formulas shown in Eqs. (14) and (15), and the maximal error is

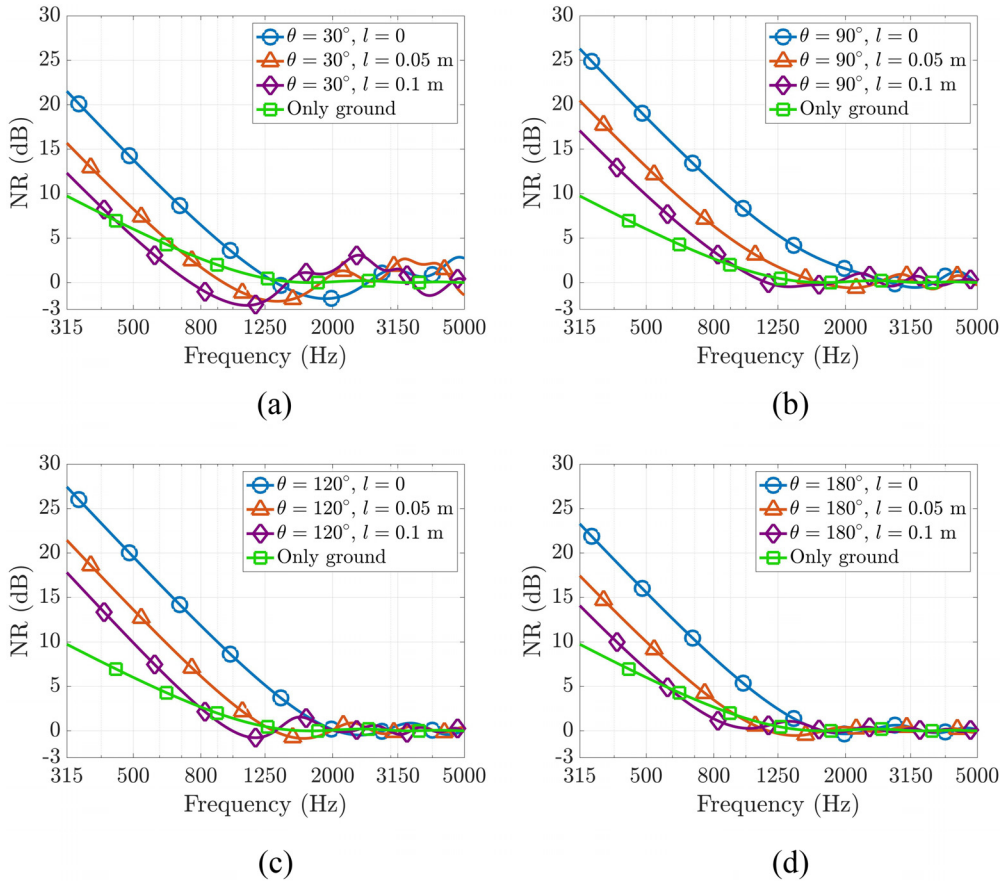

FIG. 2. (Color online) Comparisons of the noise reduction of the ANC systems with a vertically placed wedge-shaped reflector at different distances from the surfaces (a) $\theta = 30°$, (b) $\theta = 90°$, (c) $\theta = 120°$, and (d) $\theta = 180°$.

less than 0.5 dB at 500 Hz. The estimation error is caused by truncating the order not less than $(kd)^6$.

To investigate the optimal angles at different source intervals (or different frequencies), the noise reduction of the ANC system as a function of the source interval normalized to the wavelength, d/λ, and the included angle, θ, is shown in Fig. 5. It can be found that when the source interval is small compared with the wavelength, the optimal angle decreases with the source interval and the frequency. The optimal angle is between 114° and 146° when $0.01 < d/\lambda < 0.25$, and its value can be estimated by a simple formula shown in Eq. (17) within a maximal error of 5°.

In the very low frequency range, the source strength of the secondary source under optimal control is approximately opposite to that of the primary source, so the primary and secondary sources on ground can be approximately treated

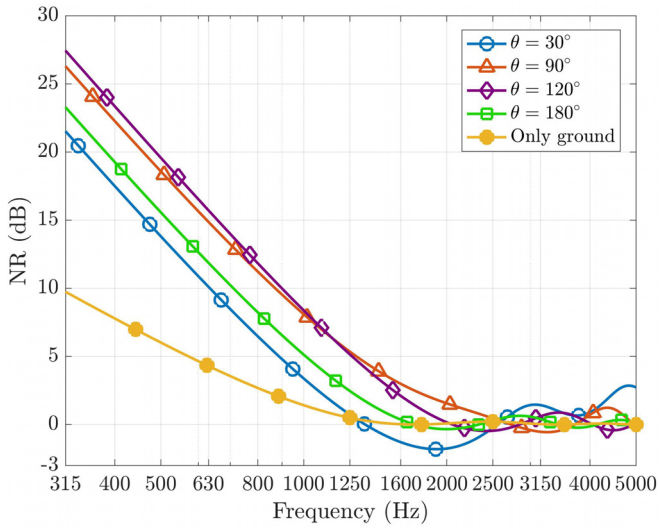

FIG. 3. (Color online) Noise reduction of the ANC system with a vertically placed wedge-shaped reflector with different included angles θ.

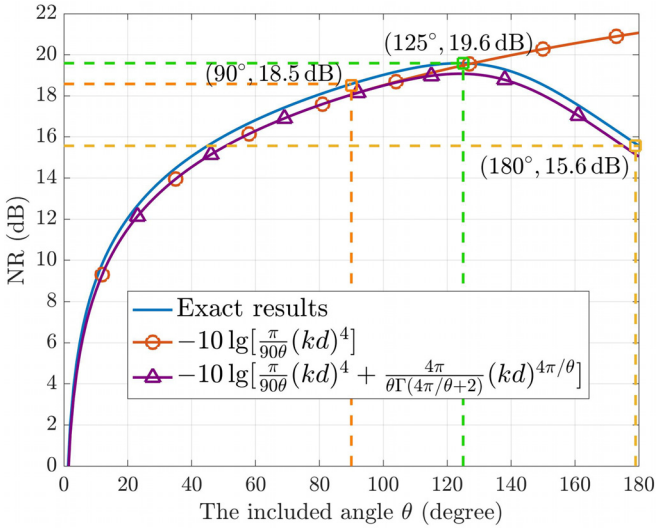

FIG. 4. (Color online) Noise reduction of the ANC system at 500 Hz with a vertically placed wedge-shaped reflector as a function of the included angles θ.

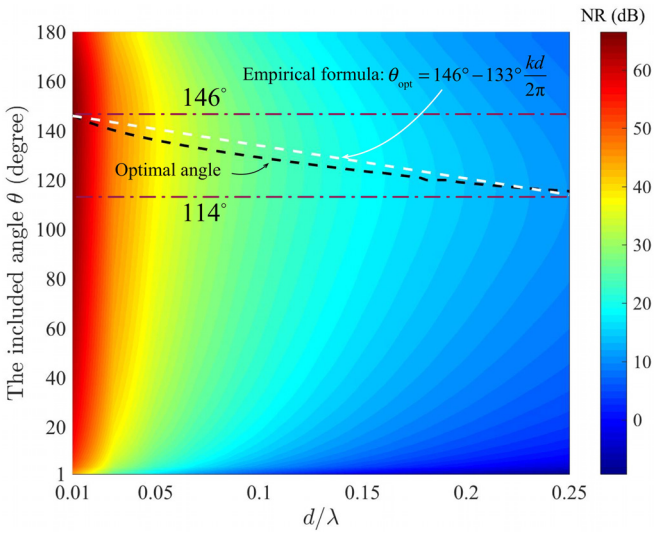

FIG. 5. (Color online) Noise reduction of the ANC systems with a vertically placed wedge-shaped reflector with different source intervals, d, and the included angles, θ.

as a pair of dipole sources with doubled source strength. When a point monopole radiates sound waves inside a wedge-shaped reflector, the total sound pressure at any field point in space consists of the direct sound and the reflected sound, which is caused by the reflections of the reflecting surface. Figure 6 shows the image source model of the ANC system with a vertically placed wedge-shaped reflector with different included angles θ in a top view, where the circles marked with "+" are the primary source and its image sources, and those marked with "−" are the secondary source and its images. When the included angle is 180°, the reflected sound of the original source is equal to the sound generated by an image source which is located at the mirror location of the original source regarding the reflecting surface. When the included angle is 120°, the reflected sound is equal to the sound generated by two image sources mirrored by each reflecting surface. When the included angle (θ) of the wedge-shaped reflector is small but is a divisor of 360°, such as 30°, 45°, 60°, and 90°, the image sources of higher orders are introduced, and there are ($360°/\theta$ – 1) image source pairs of the primary and secondary sources that are distributed evenly on the perimeter of a circle with a radius of d and centered at the secondary source.[17] For example, the total number of image sources is 11, 7, 5, 3, 2, and 1 when the included angle θ is 30°, 45°, 60°, 90°, 120°, and 180°, respectively.

The radiation power of the ANC system is the total radiation power from both primary and secondary sources. As the included angle decreases, the number of image sources of primary and secondary sources increases, the distance between each pair of primary and secondary sources (d) remains the same, and the distance between the primary (or secondary) source and its image source decreases. The additional generated image sources affect the radiation of the primary source. Specifically, the radiation is enhanced by the additional image sources of the primary source and decreased by additional image sources of the secondary source. If the distance between the primary source and its image source is larger than that of the primary source and the image source of the secondary source, the effects of the enhancement of radiation are more significant, and the noise reduction can then be increased.

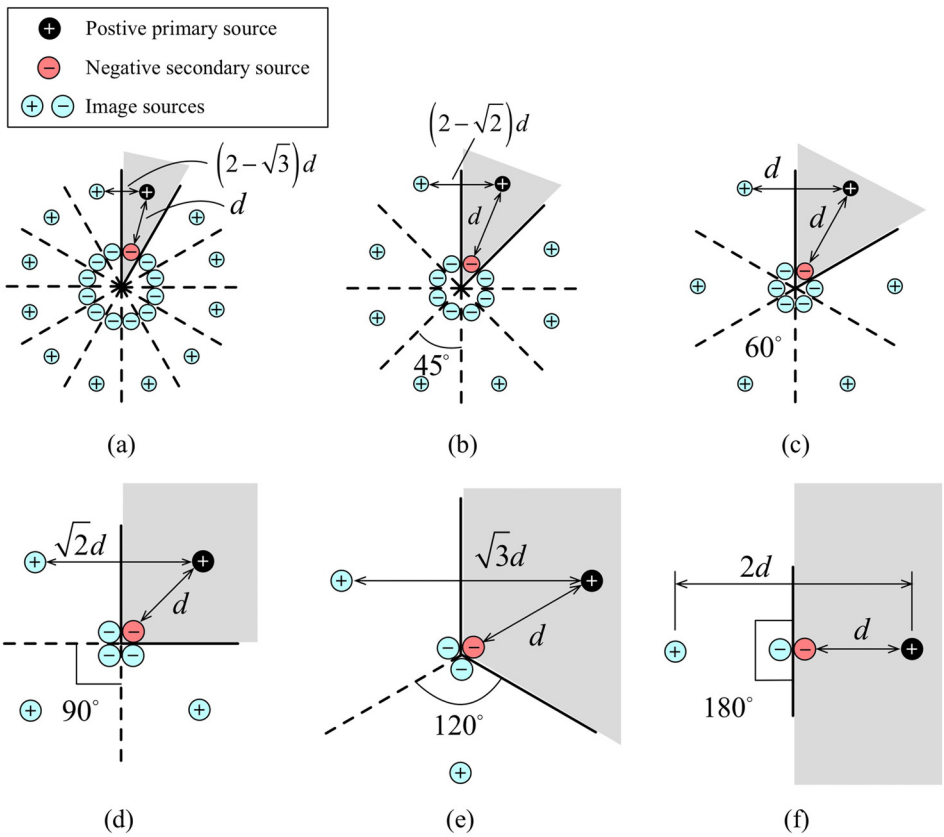

FIG. 6. (Color online) Image source model of the ANC system at low frequency with a vertically placed wedge-shaped reflector with different included angles θ (in a top view, and the sources are on the ground plane) (a) $\theta = 30°$, (b) $\theta = 45°$, (c) $\theta = 60°$, (d) $\theta = 90°$, (e) $\theta = 120°$, and (f) $\theta = 180°$.

For example, compared with the configuration with the included angle 180° where only one image source pair exists, the configuration with 120° has one more image source pair. The noise reduction of the system for the latter configuration (120°) is then higher because the distance between the primary source and its image sources, $\sqrt{3}d$, is larger than the source interval, d. When the included angle decreases to 30°, the number of image sources of the primary source is 11, and the distance between the primary source and its nearby image source is $(2-\sqrt{3})d$, which is smaller than the ANC source interval d. The reinforcing effect of the image sources of the primary source is greater than the controlling effect of the image sources of the secondary source, so the noise reduction decreases.

When the size of the reflecting surfaces is finite, there are many geometry configurations for different widths and heights, and this paper focuses on the square reflecting surface to discuss the effects of the finite size reflector. In the simulations, the included angle, θ, is set to 120° to achieve the almost optimal controlling performance, and the width (or height) of the reflector is set to 0.05 m, 0.1 m, 0.15 m, and 0.2 m. The distance between the secondary source and the intersection of the wedge-shaped reflector and the ground, l, is set to 0.01 m to avoid potential singularity of the numerical computations, and the source interval, d, is then set to 0.09 m.

Figure 7 shows the noise reduction of the ANC system with the finite-size reflecting surfaces, where the noise reduction generally increases with the reflector size and tends to that with the infinitely large reflector. For example, the noise reduction at 500 Hz is 6.8 dB without the reflector, and it can be increased by 4.3 dB, 8.0 dB, 12.0 dB, and 14.9 dB after introducing a wedge-shaped reflector with the width (or height) of 0.05 m, 0.1 m, 0.15 m, and 0.2 m, respectively. However, at some frequency ranges, the noise reduction with the finite-size reflecting surfaces can be larger than that with the infinitely large one. For example, this noise reduction of the system with a reflector with a width and height of 0.2 m is 2.8 dB larger than the infinitely large one around 600 Hz.

The numerical results show that this superior frequency occurs when the width/height of the reflector is around 0.35λ. The mechanism of the noise reduction enhancement is that the diffraction of the edge of the reflector has the maximal constructive effects with the direct wave at this specific frequency (even greater than that caused by the infinitely large reflector), so it enhances the coupling between the primary and secondary sources.

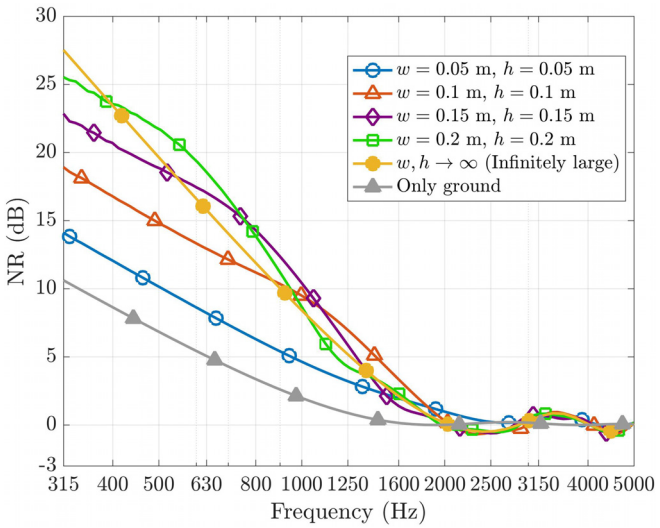

FIG. 7. (Color online) Comparisons of the ANC system with a vertically placed wedge-shaped reflector with different sizes, where $\theta = 120°$.

IV. EXPERIMENTS

The experiments with a single channel ANC system were conducted at Nanjing University in a full anechoic room with dimensions of 11.4 m × 7.8 m × 6.7 m. The sketch and photographs of the experimental setups are shown in Figs. 8 and 9, respectively. The infinitely large ground was approximated by a 3.6 m × 3.6 m wooden plate, and two 1.2 m × 1.2 m wooden plates were used to approximate the two infinitely large and vertically placed reflecting surfaces with an included angle (the wedge-shaped reflector). All the wooden plates used in the experiments have a thickness of 1.8 cm and a surface density of 15.30 kg/m^2. The ratio of the sound power reflected from the wooden plate to the total sound power radiated from the sound source is larger than 96.6% above 100 Hz, so this setup can approximate rigid surface reflections.[18]

The sound power of the system was measured with ten measuring microphones, as shown in Fig. 9(a) according to the ten positions listed in ISO 3744.[19] The sound pressure at measuring microphones was sampled with a B&K PULSE system (Nærum, Denmark) and the fast Fourier transform (FFT) analyzer in PULSE LabShop was used to obtain the FFT spectrum. Both primary and secondary sources are customized loudspeakers, and each one was made by assembling a 1-in. loudspeaker unit in a 48 mm (length) × 48 mm (width) × 38 mm (depth) Plexiglas box. The sound center of the loudspeaker was considered as the geometric center of the diaphragm of the loudspeaker. The distance between the sound centers of the primary and secondary loudspeakers was set to 0.1 m for the two infinitely large reflecting surfaces and 0.09 m for the finite size ones in the experiments to be consistent with the simulations in Sec. III.

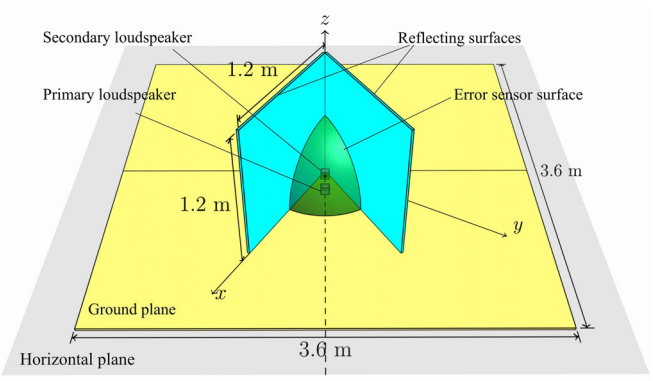

FIG. 8. (Color online) Sketch of the experiment setup, where the included angle of the two reflecting surfaces is $\theta = 60°$.

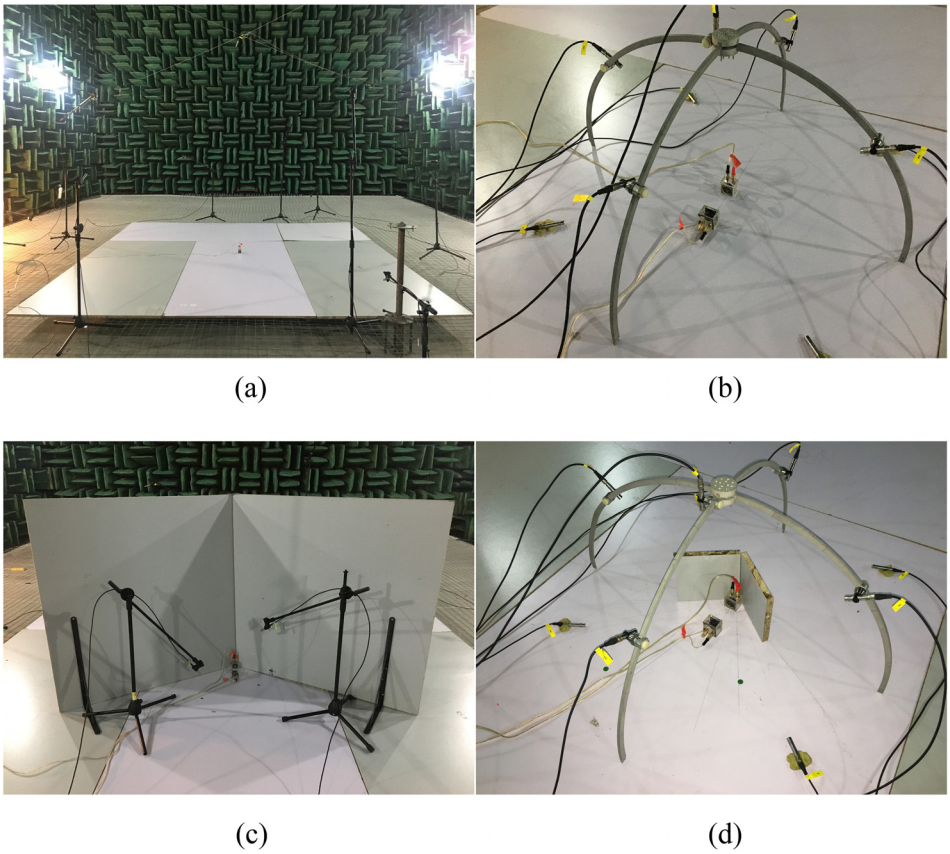

FIG. 9. (Color online) Photographs of the experimental setup: (a) the ground plane approximated by a 3.6 m × 3.6 m wooden plate and the ten measuring microphones, (b) a single channel ANC system on ground with nine error microphones, (c) a single channel ANC system on ground with two vertically placed reflecting surfaces (1.2 m × 1.2 m) and two error microphones, (d) a single channel ANC system on ground with two vertically placed reflecting surfaces (0.15 m × 0.15 m) and nine error microphones.

A commercial active noise controller (Antysound Tiger ANC WIFI-M, Nanjing, China) embedded with the waveform synthesis algorithm was used for control.[20] The internally synthesized signal at preset frequencies was used to drive the primary source and adopted as the reference signal. Considering the frequency response of the loudspeakers and the computation capability of the controller, the experiments were conducted at a number of pure tones from 300 Hz to 2 kHz with an interval of 50 Hz.

Although the goal of this research is to minimize the sound power of the system, the controller minimizes the summation of the square of the sound pressure at error microphones in the experiments. This makes the sound power noise reduction obtained in the experiment (NR_{prs}) less than NR_w, which is obtained by minimizing the sound power theoretically. For the case without additional reflecting surfaces (only ground) and the case with two finite size reflecting surfaces, the number and location of the error microphones were obtained by simulations and given in Table I. A semispherical support frame with a radius of 0.5 m centered at the secondary source was used to install the error microphones. Further simulations (not presented in this paper) by the authors show that the difference between the sound power reduction obtained by minimizing the sum of the square of the sound pressure at these error microphones arrangements and the one by minimizing the sound power theoretically is less than 0.5 dB in the frequency range from 300 Hz to 2 kHz.

TABLE I. Locations of the error microphones in the experiments for the case without additional reflecting surfaces (only ground) and the case with two finite size reflecting surfaces at the included angle 120°.

Number of the error microphone i	1	2	3	4	5	6	7	8	9
Zenith angle (°)	0	45	45	45	45	90	90	90	90
Azimuth angle (°)	0	330	60	150	240	15	105	195	285

For the case with two infinitely large reflecting surfaces, it is not convenient to install the semispherical support frame as in the former case. Therefore, the genetic searching algorithm was employed to optimize the locations of two error microphones to maximize the noise reduction.[21] In the optimization, the mean value of the difference of noise reductions, i.e., $NR_w - NR_{prs}$, at all the frequencies is chosen as the fitness function, and all the error microphones are restricted on a partially spherical surface centered at the secondary loudspeaker with a radius of 0.5 m, as shown in Fig. 8.

The optimal locations of error microphones for finite size reflecting surfaces with different included angles were obtained after genetic searching and given in Table II. Further simulations (not presented in this paper) by the authors show that both the mean value and maximal difference between the sound power reduction NR_{prs} and NR_w are less than 0.1 dB at the frequencies ranging from 300 Hz to 2 kHz with an interval of 50 Hz. Because there are also other factors in the experiments, the final optimal locations of the error microphones used in the experiments are not exactly the same as those listed in Table II, but were chosen by a process of trial and error to maximize NR_{prs} near the locations given in Table II.

The measured noise reduction, defined as the measured sound power level with the two reflecting surfaces under

TABLE II. Locations of the error microphones in the experiments for the case with two infinitely large reflecting surfaces.

	Error microphone 1		Error microphone 2	
Included angle θ (°)	Azimuth angle (°)	Zenith angle (°)	Azimuth angle (°)	Zenith angle (°)
50	47.2	36.6	25.0	81.8
60	30.0	37.5	10.2	79.0
70	4.8	36.8	17.5	81.2
80	40.1	36.8	17.9	80.7
90	38.4	35.9	19.6	84.0
100	72.1	74.8	19.4	39.2
110	34.0	72.8	101.9	40.1
120	101.2	39.8	34.1	73.3
130	36.4	73.5	20.9	39.8
140	98.0	71.0	16.4	41.1
150	46.0	70.3	15.8	41.7
160	14.6	43.3	108.3	67.5
170	154.5	44.9	114.2	66.4
180	161.5	42.0	52.3	83.8

optimal control subtracting from the one without the reflecting surfaces (only ground) and without ANC, is shown in Fig. 10. Because the loudspeaker is finite size and cube-shaped, the distance between the sound center of the secondary loudspeaker and the intersection line of the two reflecting surfaces cannot be zero and is set to 0.05 m, 0.1 m, and 0.15 m. It can be observed that the experimental results are generally in accordance with the simulation results, and the noise reduction is larger when the distance between the secondary source and the vertical reflector becomes smaller at the frequency less than approximately 900 Hz for $\theta = 120°$ or 800 Hz for $\theta = 180°$. The experimental result of the noise reduction at 300 Hz is less than the one at 350 Hz, which is not the same as that in the simulations. This might be caused by the poor low frequency response of the loudspeakers used in the experiments.

The measured noise reduction at 400 Hz and 500 Hz with the two reflecting surfaces (1.2 m × 1.2 m) when the distance l is 0.05 m is presented in Fig. 11. Due to the installation limitation in the experiments, the included angle of the two reflecting surfaces is set from 45° to 180° with an interval of 5°. The variation of experimental results is generally in accordance with that of the simulation results. But there are some differences at small included angles. For example, when the included angle is 45°, the noise reduction of the system in the experiments for 400 Hz is 11.0 dB, which is 2.6 dB less than that in the simulations. Three reasons maybe account for the differences. First, the sound field is more directional at small included angles, so the measured noise reduction may differ with the real one. Second, the near field sound is more complicated at small included

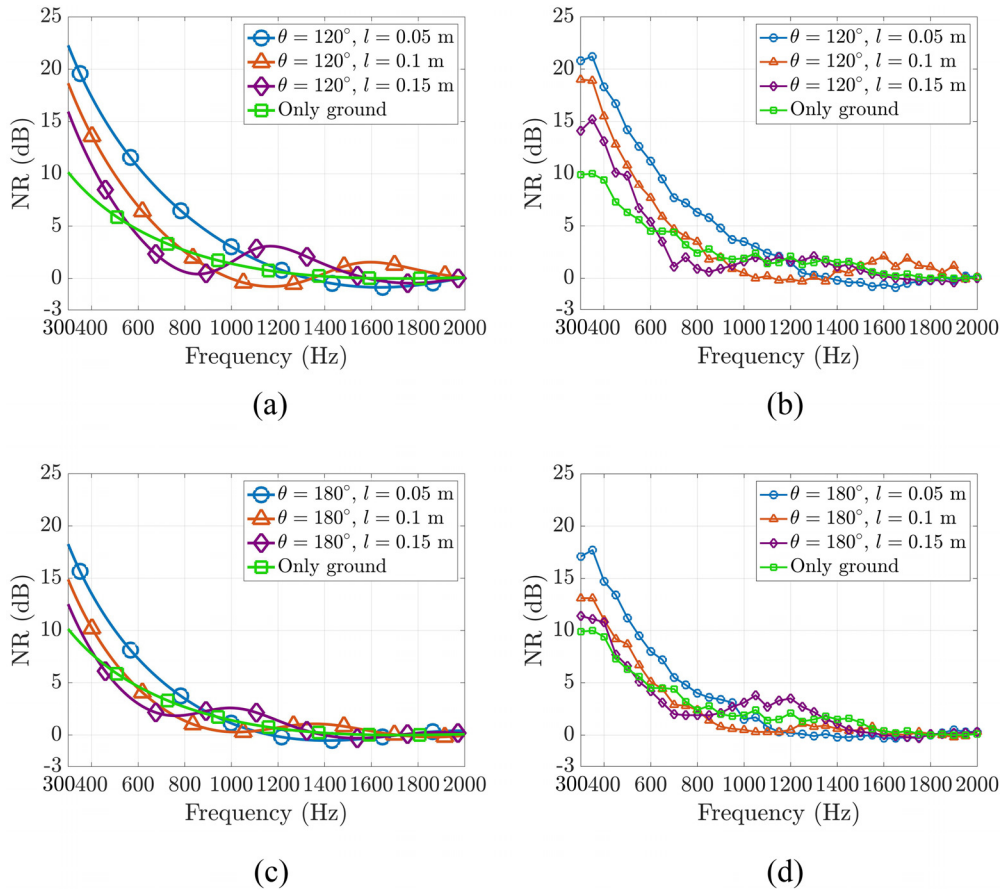

FIG. 10. (Color online) Comparisons of the noise reduction of the ANC system with two vertically placed reflecting surfaces at different distances from the surfaces: (a) simulation results for $\theta = 120°$, (b) experimental results for $\theta = 120°$, (c) simulation results for $\theta = 180°$, and (d) experimental results for $\theta = 180°$.

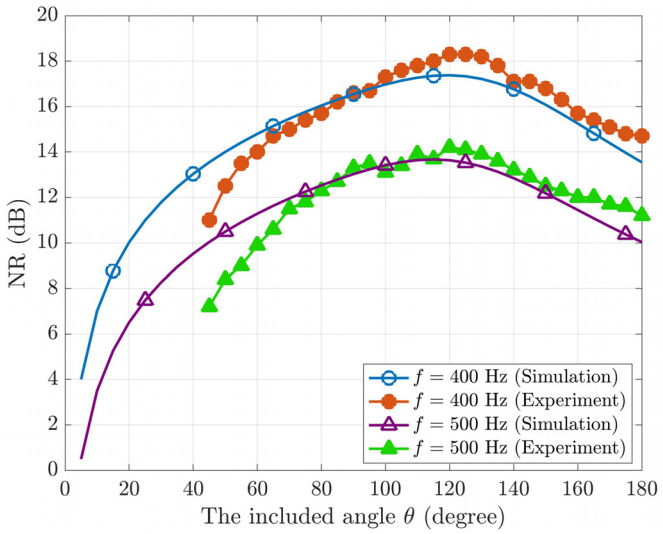

FIG. 11. (Color online) Noise reduction of the ANC system at 400 Hz and 500 Hz with two vertically placed reflecting surfaces with different included angles θ.

angles, so the optimal position of the error microphones is difficult to accurately locate. Finally, the effects of the wedge-shaped reflector reduce at small included angles because the distance between the sound center of the secondary loudspeaker and the intersection line of the two reflecting surfaces increases more than 0.05 m due to the finite size of the frame of real loudspeakers.

Figure 11 shows that the noise reduction of the ANC system increases as the angle increases from 45° and decreases as the angle increases after it achieves its maximal value at 120° for both 400 and 500 Hz in the experiments. For example, the maximal noise reduction of the ANC system at 400 Hz and 120° is 18.3 dB, which is 1.7 dB and 3.6 dB more than those of the two typical configurations with the angles 90° and 180°, respectively.

The measured noise reduction with two finite size reflecting surfaces, 0.1 m × 0.1 m or 0.2 m × 0.2 m, at different frequencies is shown in Fig. 12. The experimental results are generally in accordance with the simulation results. Better noise reduction can be achieved at certain frequencies with two finite size reflecting surfaces compared to that with the infinitely large ones. For example, the noise reduction improvement at 550 Hz by introducing two reflecting surfaces with the size 0.2 m × 0.2 m is 3.8 dB higher compared with the case where the large ones with the size 1.2 m × 1.2 m and the noise reduction improvement around 1300 Hz by introducing two reflecting surfaces with the size 0.1 m × 0.1 m is approximately 2 dB.

V. CONCLUSIONS

This paper demonstrates that the noise reduction of a single channel ANC system on ground can be significantly increased by introducing a wedge-shaped reflector after optimizing the distance between the secondary source and the reflector, the included angle, and size of the reflector. The performance improvement at the optimal included angle comes from the fact that the sound radiation reinforcement

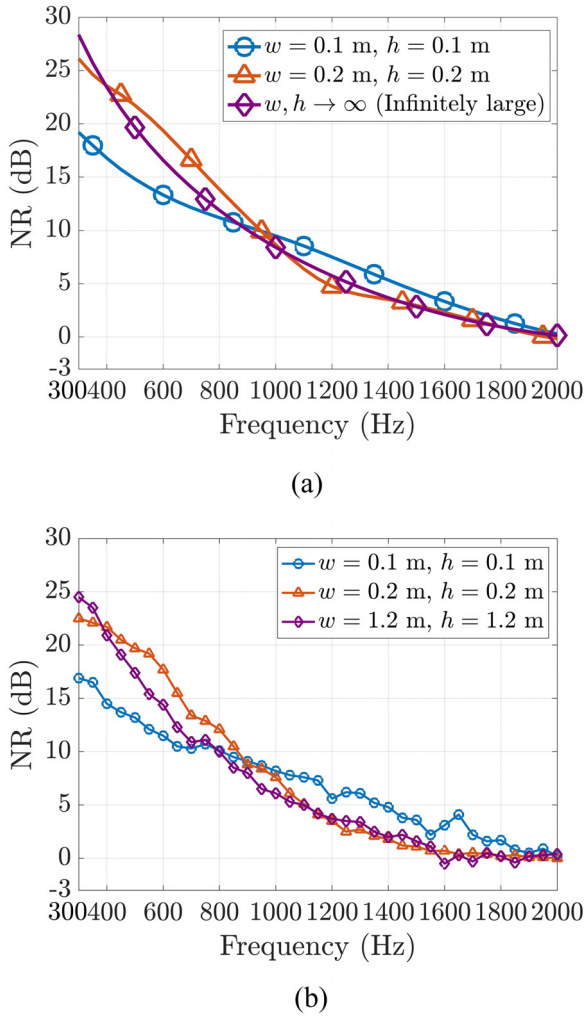

FIG. 12. (Color online) Noise reduction of the ANC system with two vertically placed reflecting surfaces with finite size and an included angle $\theta = 120°$: (a) simulation results and (b) experimental results.

of the image sources of the primary source is less than the controlling effect of the image sources of the secondary source. The performance improvement with the optimal size of the reflector comes from the increased sound pressure diffracted by the edge of the reflector at the primary source location generated by the secondary source. To maximize the noise reduction performance of such a system, the vertically placed reflector should be positioned as close as possible to the secondary source, and the included angle of the reflector should be set to approximately 125° with the size of the reflector being approximately 0.35 of the wavelength of the noise to be controlled.

The causality condition in the work is not taken into account because the noise source is assumed to be tonal. When the primary source generates the transient noise component (e.g., impact noise) or random noise (due to flow), the ANC system (shown in Figs. 1 and 6) should still be able to work if the feedforward control system is used and the reference signal can be obtained in advance. However, if the reference signal cannot be obtained in advance or the latency of the control system is too large, the real time ANC system might fail. The mechanism for active sound radiation control is to reduce the radiation impedance of the primary source

by matching the transfer functions of the acoustic paths in the system, which change little even though the signal from the source varies significantly with time. Therefore, ANC systems can deal with the transient noise and random noise in principle; however, real-time implementation must take the causality into account. Further research includes exploring the causality condition and application for the transient or random noise source with a vertical wedge-shaped reflector and the optimal configuration of the error microphones and secondary sources for multiple channel ANC systems.

ACKNOWLEDGMENTS

This research was supported by the National Science Foundation of China (Grant Nos. 11874218 and 11874219).

[1]X. Qiu, J. Lu, and J. Pan, "A new era for applications of active noise control," in *Proceedings of Inter-noise 2014*, Melbourne, Australia (2014).
[2]S. Boodoo, R. Paurobally, and Y. Bissessur, "A review of the effect of reflective surfaces on power output of sound sources and on actively created quiet zones," Acta Acust. Acust. **101**, 877–891 (2015).
[3]U. Ingard and G. L. Lamb, "Effect of a reflecting plane on the power output of sound sources," J. Acoust. Soc. Am. **29**, 743–744 (1957).
[4]D. A. Bies, "Effect of a reflecting plane on an arbitrarily oriented multipole," J. Acoust. Soc. Am. **33**(3), 286–288 (1961).
[5]K. A. Cunefare and S. Shepard, "The active control of point acoustic sources in a half-space," J. Acoust. Soc. Am. **93**(5), 2732–2739 (1993).
[6]J. Pan, X. Qiu, and R. Paurobally, "Effect of reflecting surfaces on the performance of active noise control," in *Proceedings of ACOUSTICS 2006*, Christchurch, New Zealand (2006).
[7]J. Zhong, J. Tao, and X. Qiu, "Increasing the performance of active noise control systems on ground with a finite size vertical reflecting surface," Appl. Acoust. **154**, 193–200 (2019).
[8]W. S. Shepard, Jr. and K. A. Cunefare, "Active control of extended acoustic sources in a half-space," J. Acoust. Soc. Am. **96**(4), 2262–2271 (1994).
[9]J. Tao, S. Wang, X. Qiu, and J. Pan, "Performance of a multichannel active sound radiation control system near a reflecting surface," Appl. Acoust. **123**, 1–8 (2017).
[10]J. Xue, J. Tao, and X. Qiu, "Performance of an active control system near two reflecting surfaces," in *Proceedings of 20th International Congress on Aound and Vibration*, Bangkok, Thailand (2013).
[11]J. J. Bowman, T. B. A. Senior, and P. L. E. Uslengthi, *Electromagnetic and Acoustic Scattering by Simple Shapes* (North-Holland, Amsterdam, 1969), pp. 272–275.
[12]M. J. Buckingham and A. Tolstoy, "An analytical solution for the benchmark problem: The 'ideal' wedge," J. Acoust. Soc. Am. **87**(4), 1511–1513 (1990).
[13]S. Zhao, X. Qiu, and J. Cheng, "An integral equation method for calculating sound field diffracted by a rigid barrier on an impedance ground," J. Acoust. Soc. Am. **138**(3), 1608–1613 (2015).
[14]P. A. Nelson and S. J. Elliott, *Active Control of Sound* (Academic, London, 1992), Chap. 8.
[15]P. A. Nelson, A. R. D. Curtis, S. J. Elliott, and A. J. Bullmore, "The minimum power output of free field point sources and the active control of sound," J. Sound Vib. **116**(3), 397–414 (1987).
[16]S. Zhang and J. Jin, *Computation of Special Functions* (Wiley, New York, 1996), Sec. 3.3.
[17]R. V. Waterhouse, "Radiation impedance of a source near reflectors," J. Acoust. Soc. Am. **35**(8), 1144–1151 (1963).
[18]K. Yamada, H. Takahashi, and R. Horiuchi, "Theoretical and experimental investigation of sound power transmitting through reflecting plane with low surface density in the calibration of reference sound sources," Acoust. Sci. Tech. **36**(4), 374–376 (2015).
[19]ISO 3744:2010, "Acoustics—Determination of sound power levels and sound energy levels of noise sources using sound pressure—Engineering methods for an essentially free field over a reflecting plane (International Organization for Standardization, Geneva, Switzerland, 2010).
[20]X. Qiu and C. H. Hansen, "An algorithm for active control of transformer noise with on-line cancellation path modelling based on the perturbation method," J. Sound. Vib. **240**(4), 647–665 (2001).
[21]C. Houck, J. Joines, and M. Kay, "A genetic algorithm for function optimization: A MATLAB implementation," Technical Report No. 09-95, NCSU-IE (1995).